Journal of Theoretical Biology 310 (2012) 164–174

Contents lists available at SciVerse ScienceDirect

Journal of Theoretical Biology

journal homepage: www.elsevier.com/locate/yjtbi

An algorithm for the simulation of the growth of root systems on deformable domains

Lionel Xavier Dupuy [a,*], Matthieu Vignes [b]

[a] The James Hutton Institute, Invergowrie, Dundee DD2 5DA, Scotland
[b] UR875 UBIA, INRA, 31326 Castanet-Tolosan Cedex, France

HIGHLIGHTS

- We model the growth of root systems using density functions on deformable domains.
- Growth is modelled using PDE and root trajectories are used to deform the domain.
- We showed root domains can be predicted using developmentally meaningful parameters.
- Deformable domains are computationally efficient and can be used in population models.

ARTICLE INFO

Article history:
Received 21 September 2011
Received in revised form
8 June 2012
Accepted 17 June 2012
Available online 23 June 2012

Keywords:
Density models
PDE
Deformable domain
Root architecture
Barley

ABSTRACT

Models of root systems are essential tools to understand how crops access and use soil resources during their development. However, scaling up such models to field scale remains a great challenge.

In this paper, we detail a new approach to compute the growth of root systems based on density distribution functions. Growth was modelled as the dynamics of root apical meristems, using Partial Differential Equations. Trajectories of root apical meristems were used to deform root domains, the bounded support of root density functions, and update density distributions at each time increment of the simulation.

Our results demonstrate that it is possible to predict the growth of root domains, by including developmentally meaningful parameters such as root elongation rate, gravitropic rate and branching rate. Models of this type are computationally more efficient than state-of-the-art finite volume methods. At a given prediction accuracy, computational time is over 10 times quicker; it allowed deformable models to be used to simulate ensembles of interacting plants. Application to root competition in crop–weed systems is demonstrated.

The models presented in this study indicate that similar approaches could be developed to model shoot or whole plant processes with potential applications in crop and ecological modelling.

1. Introduction

Plant architectures are involved in key biological and environmental processes (Fourcaud et al., 2008). Root architectures in particular are optimised to capture and assimilate large amounts of water and mineral elements from the soil, thereby contributing to crop yield and effective food production (Lynch, 2007). Root architectures also protect soils against erosion and other forms of land degradation (Stokes et al., 2009). Due to their inherent multifunctional nature, root architectures are difficult to understand intuitively. Thus, models are of utmost importance to analyse the complexity of root architectures and their functions.

Root architectures result from the organised expansion of a multitude of apical meristems (root tips), which develop in a series of elongation and initiation events. Current models use computer simulations to mimic these processes. The geometry of roots and their arrangement within the root system are assembled iteratively from a set of virtual apical meristems, whose activities are simulated independently from each other (Pagès et al., 2004; Wu et al., 2007; Lucas et al., 2011). Root architectural models can, in turn, be used to make predictions on water and nutrient uptake by coupling growth to physical models (Ge et al., 2000; Doussan et al., 2006; Zhang et al., 2007; Wiegers et al., 2009).

Unfortunately, for root architectural models it has proved to be difficult to define their parameters and assign them values (Tsegaye et al., 1995). They also require sophisticated algorithms, in order to be coupled to soil models (Draye et al., 2010; Leitner et al., 2010). Simplified approaches, such as root density models, could be used to overcome these shortcomings. Density-based models aggregate root properties into root distribution functions. Changes with time of density distribution functions can then be modelled empirically, for example using sliding exponential

* Corresponding author. Tel.: +44 1382 568521; fax: +44 8449 285429.
E-mail address: lionel.dupuy@hutton.ac.uk (L.X. Dupuy).

0022-5193/$ - see front matter © 2012 Elsevier Ltd. All rights reserved.
http://dx.doi.org/10.1016/j.jtbi.2012.06.025

profiles (Gerwitz and Page, 1974; King et al., 2003) or mechanistically using partial differential (Acock and Pachepsky, 1996; Bastian et al., 2008). In the latter case, analytical methods can provide simple growth functions (de Willigen et al., 2002; Schnepf et al., 2008). Approximated numerical solutions can also be obtained to analyse more complex systems (Reddy and Pachepsky, 2001). However, density-based models were seldom used to model ensembles of interacting plants. One remaining challenge is to limit the number of unknowns in numerical simulations, so that solutions can be obtained by standard desktop computers.

This paper presents a density-based approach to model ensembles of root systems in the field. The root system is defined as a deformable domain and density distribution functions are used to model the distribution of roots within this domain. We expanded the system of differential equations introduced in a previous work (Dupuy et al., 2010), which proposed an Eulerian solver, and developed a Lagrangian approach to solve equations on 3D deformable grids. The performance of our solver was compared to results obtained in a two-dimensional setting, where the conservation equation could be solved analytically. Finally, a simple case of crop–weed competition was studied to illustrate applications to field-based crop processes.

2. Materials and methods

2.1. A density-based framework to model root systems dynamics

In this paper, the dynamic structure of the root system is represented as a combination of density distribution functions, following the principles proposed in a previous work (Dupuy et al., 2010). First, root tip density (ρ_a) indicates regions where growth occurs. Secondly, root length density (ρ_l) is defined as the total root length per unit soil volume. Root length density is required, for example, to predict water and nutrient uptake from the soil (King et al., 2003). Finally, branching density (ρ_b), defined as the number of connections per unit soil volume, models the topology of root connections. Root density distribution functions are defined on domains that include both: (i) spatial coordinates (x,y,z) of roots in soil (Fig. 1A) and (ii) their direction of growth (Fig. 1B), which is defined in a local spherical coordinate system, more specifically gravitropic angle α and plagiotropic angle β (see Fig. 1). A root and its growth direction are therefore characterised by a point $\mathbf{m}$ in a 5-dimensional space $\mathbf{m}=(x,y,z,\alpha,\beta)\in E$, $E\subset\mathbb{R}^5$ (Fig. 1C). In this setting, a root density distribution function is a mapping $\rho: E\mapsto\mathbb{R}$ such that $\int_\Omega\int_V \rho dV\, d\Omega$ represents the total quantity of roots contained in volume V and whose growth direction

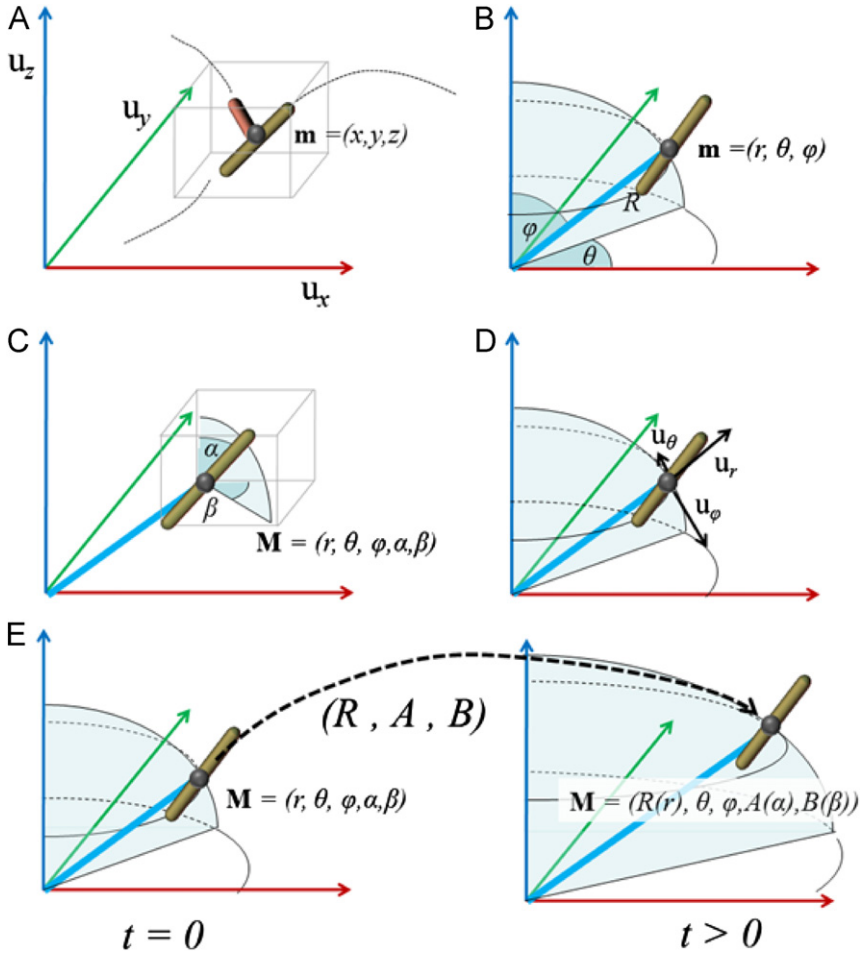

Fig. 1. Describing root systems with density distribution functions. (A) Root systems are characterised locally at point $\mathbf{M}=(x,y,z)$, by root densities (*e.g.* number of root tips or total length of root per unit volume, here depicted by brown cylinders). (B) Root coordinates can also be expressed in a spherical coordinate system, so that the position of roots $\mathbf{M}$ is defined by a radius and azimuth and zenith angles: $\mathbf{M}=(r,\theta,\varphi)$. (C) Root orientation must complement root position, so that the expansion of the root system can be predicted. The coordinate system is therefore expanded to record the direction of roots. Root direction in the spherical coordinate system is defined by inclination and azimuth angles (α,β). (D) A spherical coordinate system defines a local basis $(\mathbf{u_r},\mathbf{u_\theta},\mathbf{u_\varphi})$, and hence allows the modelling of deformations of the root domain. (E) In a Lagrangian setting, material coordinates of a reference state is defined at $t=0$, so that $\mathbf{M}=(r,\theta,\varphi,\alpha,\beta)$. The deformed state, which results from the growth of the root system, is then expressed as a function of the reference state $\mathbf{M}=(R(r),\theta,\varphi,A(\alpha),B(\beta))$. (For interpretation of the references to color in this figure caption, the reader is referred to the web version of this article.)

is enclosed in the solid angle Ω. The growth of the root system is then expressed through the activity of its apical meristems, and the following conservation equation is obtained:

$$\frac{\partial \rho_a}{\partial t} + \nabla \cdot (\mathbf{v}\rho_a) = b, \tag{1}$$

where $\nabla = (\partial/\partial x, \partial/\partial y, \partial/\partial z, \partial/\partial \alpha, \partial/\partial \beta)$ is the gradient operator defined on E. $\mathbf{v} = (e\cos\beta\sin\alpha, e\sin\beta\sin\alpha, e\cos\alpha, g, h)$ is the advection velocity field, where e is the root elongation rate ($\mathrm{cm\,day^{-1}}$) and $e\cos\beta\sin\alpha$, $e\sin\beta\sin\alpha$ and $e\cos\alpha$ are the projections of the velocity vector on the x, y and z axes, respectively. g is the gravitropic rate ($\mathrm{day^{-1}}$) and h is the plagiotropic rate ($\mathrm{day^{-1}}$). b is a source term which accounts for the initiation of new roots through branching ($\mathrm{cm^{-3}\,day^{-1}}$). Eq. (1) is an advection equation on the generalised space E. It links the changes in root meristem density to root growth parameters, *e.g.* elongation rate e, gravitropic rate g and branching rate b.

In this study, we used the following initial density distribution functions:

$$\rho_a(\mathbf{m},0) = \mathring{\rho}_a(\mathbf{m}), \tag{2}$$

$$\rho_l(\mathbf{m},0) = 0, \tag{3}$$

$$\rho_b(\mathbf{m},0) = 0, \tag{4}$$

It is difficult to define initial conditions accurately because density distributions are less suitable to model plants at the seed stage. However, it is possible to limit the difference between modelled initial conditions and real root distribution at seedling stage. Here $\mathring{\rho}_a$ is a non-negative bounded function of $\mathbf{m}$ for which we choose a small bounded support, which localises initial growth activity near the seed. If solutions to Eq. (1) are available, root length density (ρ_l) and root branching density (ρ_b) follow by integrating root tip density and volumetric branching rate with time: $\rho_l = \int e\rho_a\, dt$ and $\rho_b = \int b\, dt$.

2.2. Deformable domains for modelling the growth of root systems

In most cases, it is not possible to derive exact solutions to Eq. (1). Numerical techniques are needed to obtain approximate predictions. Finite volume methods, for example, decompose the distribution function on a discrete grid of the physical space. On such grids, unknowns are the average values of the distribution function in control volumes of the grid, which are termed cells. Because the set of cells in the grid is finite, it is possible to compute fluxes of root tips, which enter and leave each cell of the grid at a given stage of the simulation. This allows an approximate solution to be constructed incrementally from a set of initial conditions. As the number of cells in the grid increases, the error of discretisation diminishes and the accuracy of the solution is improved. The convergence rate of a method is the speed at which the numerical approximation approaches the exact solution.

Fixed grids, used to compute fluxes of matter between adjacent cells, are generally referred to as Eulerian. Eulerian descriptions are widely used in many areas of physical sciences including fluid mechanics and were applied to root models by Bastian et al. (2008). Alternatively, deformable grids can be used to assign physical quantities to a given material cell of the grid. Such methods are termed Lagrangian, and are widely used in solid mechanics (Zienkiewicz and Taylor, 1998). Lagrangian descriptions are well adapted to plant models, because plants have solid tissues and their growth is slow and tractable. We will term such models Continuous Deformable Plant Models (CDPMs).

In a Lagrangian setting, coordinates $\mathbf{M}$ of a material point are no longer considered as constant and vary as a function of time and initial conditions $\mathbf{m}$ such that $\mathbf{M} = \mathbf{M}(\mathbf{m},t)$. We use capital letters to indicate coordinates of material point. In order to be able to compute deformation of the root domain, we made the three following hypotheses:

- H1 plant coordinate system: positions in the root system are expressed in a local spherical coordinate system (Fig. 1B) centred on the seed of each plant. Each point in the three-dimensional space is defined by the distance from the seed r, its azimuth angle θ and its zenith angle φ, and it defines an associated local basis $(\mathbf{u_r},\mathbf{u}_\theta,\mathbf{u}_\varphi)$ (Fig. 1D). In order to simplify computations, we further assume that there is no flux along the tangential direction $\mathbf{u}_\theta$. Therefore, the direction of root elongation is prescribed by a gravitropic angle α, a root plagiotropic rate set to zero and the plagiotropic angle is centripetal ($\rho_a = 0$ if $\beta \neq \theta$). Eq. (1) is therefore transformed into

$$\frac{\partial \rho_a}{\partial t} + \frac{1}{r^2}\frac{e\cos(\alpha-\varphi)r^2\rho_a}{\partial r} + \frac{1}{r\sin\varphi}\frac{e\sin(\alpha-\varphi)\sin(\varphi)\rho_a}{\partial \varphi} + \frac{\partial g\rho_a}{\partial \alpha} = b. \tag{5}$$

  Although there is no flux in the tangential direction, different growth properties of the root system can be defined as a function of the azimuth. This equation is therefore defined for any $\theta \in [0, 2\pi[$. Generalisation to a full 3D model can be obtained by adding fluxes in the tangential plane to complement Eqs. (9)–(11).
- H2 semi-Lagrangian description: in order to facilitate the computation of overlapping plant domains, we apply an Eulerian description of root tip movement to azimuth and zenith angles, so that, although the domain expands radially, θ and φ remain constant during simulation. The position $\mathbf{M}$ of a material point in such a system is therefore defined as (Fig. 1E)

$$\mathbf{M} = (R(r,t),\theta,\varphi,A(\alpha,t),B(\beta,t)). \tag{6}$$

- H3 reduction of dimensionality: the angle α and the radial distance r are assumed to be independent variables. The root tip density at a given time can therefore be expressed as the product of two functions f and g such that

$$\rho_a = f(R,\theta,\varphi) \times g(\theta,\varphi,\alpha), \tag{7}$$

  f describes the root tip density at a given position in space and constitutes the primary description of the root system, while g defines the probability distribution of root inclination angle.

The spatial domain of a root system is decomposed into a grid of cells with a fixed number of subdivisions in each of the dimensions of the coordinate system. We therefore define n_R, n_θ and n_φ as the number of cells along the coordinate lines of the mesh, respectively, radial, azimuth, and zenith angle coordinates. The size of a cell is defined by fixed angular increments $\Delta\theta, \Delta\varphi$ and a variable length in the radial direction ΔR. The spatial coordinates of a cell in the grid can therefore be based on three indices (i,j,k) such that the coordinates $(R_{ijk},\theta_{ijk},\varphi_{ijk})$ define the spatial position of the cell C_{ijk} in the grid. For example, the zenith angle of the cell C_{ijk} is φ_{ijk}. Since the grid has cells of constant zenith angle increments φ_{ijk} is calculated as $k\Delta\varphi$. We also define the quantity $Q_{ijk} = \int_{V_{ijk}} f\, dV$, which is a close approximation of the number of roots in the cell C_{ijk}. In this cell, roots have a distribution of root inclination angle A_{ijl} with associated fraction in the cell $G_{ijl} = \int_{V_{ijl}} g\, dV$. In order to simplify notations, we present inferences for a single root inclination angle, *i.e.* $g = 1$, and generalisation is achieved by repeating the calculus for other angles. A single index will also be used to denote the coordinates of each cell: coordinates of the ith cell C_i will be denoted $\mathbf{M}_i = (R_i,\theta_i,\varphi_i,A_i)$. Cell positions and root quantities are defined at time $t = \tau\Delta t$, so that Q_i^τ indicates the average number of root

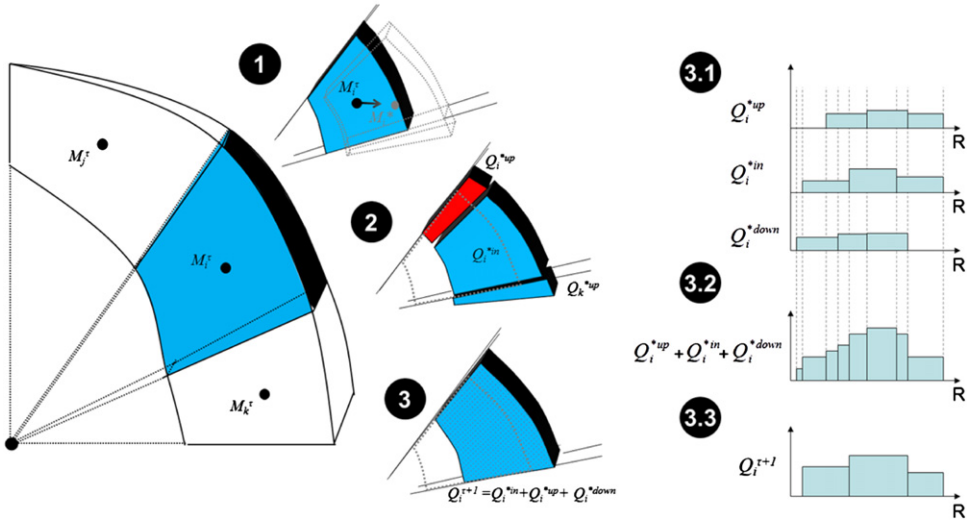

Fig. 2. Geometrical representation of the algorithm for the computation of the growth of root systems. A grid at time step τ consists of a finite set of cells, here three adjacent cells which coordinates at time step τ are $\mathbf{M}_i^\tau$,$\mathbf{M}_j^\tau$,$\mathbf{M}_k^\tau$. Calculation of the deformed mesh and corresponding root density follows in three main steps: (1) deform: trajectories of root tips are used to determine the displacement of the nodes of the grid (dashed grey lines) and result in a deformed state denoted $\mathbf{M}_i^*$. (2) Cut: root quantities in the deformed grid are decomposed into three components; Q_i^{in} the distribution of root tips staying in the current angular domain φ_i and expanding in the radial direction; Q_i^{up} the distribution of root tips entering the angular domain φ_i from the top; and Q_i^{down} the distribution of root tips entering the angular domain. In the example depicted on the figure, Q_i^{up} (in red) results from the deformation of upward cell Q_j^τ, while Q_i^{down} is equal to 0. (3) Merge: components with matching angular coordinates are assembled into the root apical meristem density distribution at time step $\tau+1$. (3.1) A collection of non-matching density distributions are obtained from the cutting step. (3.2) Expanded, upward and downward flows are decomposed into smaller matching radial bins. (3.3) The distribution of root tips at the next time step is then determined by merging the bins into a new radial distribution with the required number of bins. (For interpretation of the references to color in this figure caption, the reader is referred to the web version of this article.)

tips at time step τ in cell i. At each time step, the root domain is deformed in the radial direction, and root density values are updated according to fluxes through tangential planes of the cell (see Fig. 2). Both deformation of the grid in the radial direction and the fluxes between the control volumes are based on the characteristics of Eq. (1), which encodes trajectories of root tips through time (Mattheij et al., 2005). Each time step of the simulation is therefore decomposed into three steps

1. The characteristic equation is used to compute the deformation of the grid. Quantities defined on the deformed grid will be denoted with a star. For example, $\mathbf{M}_i^*$ defines the coordinates of the cells of the grid (Fig. 2.1). A deformed grid, with apical meristem distribution Q_i^*, is obtained using a finite difference time integration of the characteristic equation, here a forward Euler scheme

$$\mathbf{M}_i^* = \mathbf{M}_i^\tau + \mathbf{V}_i^\tau \Delta t, \tag{8}$$

where $\mathbf{V}_i^\tau$ is the root apical meristem velocity expressed in the spherical coordinate system at position $\mathbf{M}_i^\tau$: $\mathbf{V}_i^\tau = e_0 \cos(A_i-\varphi_i)\mathbf{u}_\mathbf{r} + e_0 \sin(A_i-\varphi_i)\mathbf{u}_{\boldsymbol{\varphi}} + g\mathbf{u}_{\boldsymbol{\alpha}}$.

2. At this stage, the angular coordinates of the deformed grid $\mathbf{M}_i^*$ are not uniformly distributed anymore. The displacement of the nodes in the angular coordinates φ must be transformed into fluxes entering and leaving cells in the tangential directions (Fig. 2.2). This is achieved by decomposing Q_i^* into three new distinct distributions Q_i^{*d}, $d \in \{in,up,down\}$ with matching angular coordinates. More precisely, if cells C_j and C_k are adjacent and, respectively, above and underneath C_i (see Fig. 2.1), Q_i^{*in} represents the number of roots that expand but stay in the interval $[\varphi_i-\Delta\varphi/2,\varphi_i+\Delta\varphi/2]$, Q_j^{*down} represents the number of roots that are displaced upwards in the interval $[\varphi_i-3\Delta\varphi/2,\varphi_i-\Delta\varphi/2]$ and Q_k^{*up} represents the number of roots that are displaced downwards in the interval $[\varphi_i+\Delta\varphi/2,\varphi_i+3\Delta\varphi/2]$. These quantities are calculated using the projection of the velocity of root tips on the unit vector perpendicular to a plane of constant zenith angle (Fig. 2.2).
if $\mathbf{V}_i^\tau \cdot \mathbf{u}_{\boldsymbol{\varphi}} > 0$:

$$Q_i^{*in} = Q_i^\tau\left(1-\Delta t\frac{\mathbf{V}_i^\tau \cdot \mathbf{u}_{\boldsymbol{\varphi}}}{R_i^\tau \Delta\varphi}\right)+\Delta t b \quad \text{and} \quad Q_k^{*up} = Q_i^\tau \Delta t \frac{\mathbf{V}_i^\tau \cdot \mathbf{u}_{\boldsymbol{\varphi}}}{R_i^\tau \Delta\varphi}, \tag{9}$$

if $\mathbf{V}_i^\tau \cdot \mathbf{u}_{\boldsymbol{\varphi}} < 0$:

$$Q_i^{*in} = Q_i^\tau\left(1+\Delta t\frac{\mathbf{V}_i^\tau \cdot \mathbf{u}_{\boldsymbol{\varphi}}}{R_i^\tau \Delta\varphi}\right)+\Delta t b \quad \text{and} \quad Q_j^{*down} = -Q_i^\tau \Delta t \frac{\mathbf{V}_i^\tau \cdot \mathbf{u}_{\boldsymbol{\varphi}}}{R_i^\tau \Delta\varphi}. \tag{10}$$

3. The distribution of root quantities on the mesh, at time step $\tau+1$, is determined as the sum of the number of roots that stay in cell C_i and the number of roots that enter cell C_i (Fig. 2.3)

$$Q_i^{\tau+1} = \sum_{d\,\in\,\{in,up,down\}} Q_i^{*d}. \tag{11}$$

Since the quantity of root tips entering and leaving a cell Q_i^{*d} originate from cells in distinct deformed state, they will not have matching radial distribution (Fig. 2.3.1). Cells are therefore subdivided in the radial direction, in order to obtain matching radial distribution. Root quantities are then summed (Fig. 2.3.2) and merged into a new distribution with an appropriate number of cells in the radial direction (see Fig. 2.3.3).

Steps 1–3 are repeated until $\tau\Delta t$ reaches the required duration of growth. The root length density is, in turn, determined on a distinct regular grid in the spherical coordinate with matching angular increments using a trapezoidal quadrature.

2.3. Modelling interactions with the neighbouring environment

In this section, we describe the case where s plants are growing in a 3D soil volume. The grid of the pth plant is centred

on the location of its seed at position $(x^p,y^p,0)$. Each plant defines a root length density distribution function l^p such that $l^p(\mathbf{m}) = \int \rho_l \, d\alpha$ is the root length density of plant p at position $\mathbf{m} = (r,\varphi,\theta)$ in the plant local coordinate system. In order to model interactions between plants, overlapping cells must be identified efficiently. This is achieved by expressing global positions in soil (x,y,z) in each plant local coordinate system

$$r = \sqrt{(x-x^p)^2+(y-y^p)^2+z^2}, \tag{12}$$

$$\varphi = \arccos(z/r), \tag{13}$$

$$\theta = \arctan((y-y^p)/(x-x^p)). \tag{14}$$

Functions l^p are then obtained by trilinear interpolation using root length density of neighbouring cells noted l^p_{ijk} obtained using the following formula:

$$l^p_{ijk} = l^p\left(\left(\left\lfloor\frac{r}{\Delta r}\right\rfloor+i\right)\Delta r,\left(\left\lfloor\frac{\theta}{\Delta\theta}\right\rfloor+j\right)\Delta\theta,\left(\left\lfloor\frac{\varphi}{\Delta\varphi}\right\rfloor+k\right)\Delta\varphi\right), \tag{15}$$

with $(i,j,k)\in\{0,1\}^3$ (eight combinations are possible) and $\lfloor x\rfloor$ is the floor function (its value is the largest integer inferior or equal to x).

For each point in the soil domain, it is therefore possible to define a vector of size s, the pth component of which contains the root length density of the corresponding plant. This vector is called the mixture vector $\mathbf{l}$, and is defined at all points of the soil volume. $\mathbf{l}$ is calculated using the formula:

$$\mathbf{l}(x,y,z) = \left(\sum_{(i,j,k)\in\{0,1\}^3} l^p_{ijk}\delta_i(\zeta_r)\delta_j(\zeta_\theta)\delta_k(\zeta_\varphi)\right)_{1\le p\le s}, \tag{16}$$

where $\delta_i(x) = x$ if $i=1$ and $\delta_i(x) = 1-x$ if $i=0$; $(\zeta_r,\zeta_\theta,\zeta_\varphi)$ are the relative position in the tetrahedron, *e.g.* $\zeta_r = r/\Delta r - \lfloor r/\Delta r\rfloor$. Computing Eq. (16) has complexity $O(s)$. The root length density mixture vector is a key to define interaction processes, and an example of its application is provided in the last part of the method section.

2.4. Comparing CDPM predictions with analytical solutions

It is important to ensure that the solutions obtained with the CDPM approach are satisfactory approximations of the true solutions of Eq. (1). In this section, we derive an analytical solution to Eq. (1) in a simplified two-dimensional case, so that we will be able to evaluate the accuracy of the approximate solutions that are produced by traditional algorithms and the new approach we propose. Coefficients describing root elongation rate, gravitropic rate and branching rate are defined as

$$e = e_0,$$

$$g = -g_0\alpha,$$

$$b = b_0\rho^0_a, \tag{17}$$

where $e_0 = 2$ cm day^{-1}, $g_0 = 0$ or 0.3 day^{-1} and $b_0 = 0.3$ cm^{-3} day^{-1}.

In this setting, Eq. (1) writes

$$\frac{\partial\rho^0_a}{\partial t} + e_0\sin(\alpha)\frac{\partial\rho^0_a}{\partial x} + e_0\cos(\alpha)\frac{\partial\rho^0_a}{\partial z} - \frac{\partial g_0\alpha\rho^0_a}{\partial\alpha} = 0,$$

$$\frac{\partial\rho^1_a}{\partial t} + e_0\sin(\alpha)\frac{\partial\rho^1_a}{\partial x} + e_0\cos(\alpha)\frac{\partial\rho^1_a}{\partial z} - \frac{\partial g_0\alpha\rho^1_a}{\partial\alpha} = b_0\rho^0_a. \tag{18}$$

Solutions of Eq. (18) were obtained using the method of characteristics (Mattheij et al., 2005) in a two stage process. First, trajectories of material points on the domain (here root tips) were derived by solving the characteristic equation, defined as a set of ordinary differential equations (ODE)

$$\mathbf{M}'(t) = \begin{pmatrix}\tilde{x}'(t)\\ \tilde{z}'(t)\\ \tilde{\alpha}'(t)\end{pmatrix} = \begin{pmatrix}e_0\sin\tilde{\alpha}\\ e_0\cos\tilde{\alpha}\\ -g_0\tilde{\alpha}\end{pmatrix}. \tag{19}$$

The third ODE of the system of Eqs. (19) describes the evolution of root angle with time. It is independent from the two former equations and was solved independently. Next, the first two ODEs in (19) were solved by replacing $\tilde{\alpha}$ in the first two ODEs by the solution that was just obtained from the third ODE of (19). Then sine and cosine functions were decomposed using a Taylor series expansion. Along the trajectories defined by the characteristic equation, the solution of the conservation law is expressed as an integrated ODE

$$\frac{d\rho^0_a(\mathbf{M}(t),t)}{dt} = g_0\rho^0_a(\mathbf{M}(t),t). \tag{20}$$

Combining these two equations the final solution was expressed as

$$\rho^0_a(x,z,\alpha,t) = \mathring{\rho}_a(x+x_0(t),z+z_0(t),\alpha e^{-g_0t})e^{g_0t}, \tag{21}$$

where $x_0(t)$ and $z_0(t)$ define the deformation of the initial distribution $\mathring{\rho}_a$ with time

$$x_0(t) = \sum_{k\ge0}\frac{(-1)^k\alpha^{2k+1}e_0}{g_0(2k+1)(2k+1)!}(1-e^{(2k+1)g_0t}),$$

$$z_0(t) = -e_0t + \sum_{k\ge1}\frac{(-1)^k\alpha^{2k}e_0}{2g_0k(2k)!}(1-e^{2kg_0t}). \tag{22}$$

The same principle can be applied to first order lateral roots. Since the elongation and branching rates are the same, root tips have the same characteristic equation, and along characteristic curves, the solution of the conservation law is expressed as an integrated ODE

$$\frac{d\rho^1_a(\mathbf{M}(t),t)}{dt} = g_0\rho^1_a(\mathbf{M}(t),t) + b_0\rho^0_a. \tag{23}$$

The final solution for lateral roots is then obtained as

$$\rho^1_a(x,z,\alpha,t) = b_0t\mathring{\rho}_a(x+x_0(t),z+z_0(t),\alpha e^{-g_0t})e^{g_0t}. \tag{24}$$

The error introduced by numerical approximations was characterised by the Root Mean Square Error (RMSE) computed for this grid, as a distance measure between the two distributions

$$\mathrm{RMSE} = \left(\sum_{i=1}^{n}(\rho_a(x_i,z_i,\alpha_i,\tau\Delta t) - Q^t_i)^2\right)^{1/2}. \tag{25}$$

2.5. Accuracy and convergence of CDPMs

Simulations of CPMs were performed in order to analyse the accuracy of CDPMs. For these simulations, the grid defining the root domain consisted of a fixed number of subdivisions along the R, ϕ and A coordinate lines of the mesh and only one cell along the θ azimuth coordinate line. Simulations were carried out with the following number of subdivisions 8, 16, 32, 64 and 128 cells. We then assessed convergence towards the exact solution. The choice of the time increment is set according to the Courant number (relation between time increment and cell size to maintain convergence of numerical scheme) in order to allow displacement of root meristems of velocity e_0 to be resolved in the direction $\mathbf{u}_\varphi$: $\Delta t = 0.5\min(R_i\Delta\varphi_i)/e_0$. During the course of the simulation, cells deform and the time increment varied accordingly.

We applied two standard finite volume methods, upwind and upwind with minmod flux limiter schemes (Leveque, 2002),

to obtain solutions to Eq. (18) and compare the results with those obtained using the deformable domain approach. The "upwind scheme" is a first order method which uses the direction of the propagation of the wave to compute the net flow in each cell of the grid. The "minmod scheme" is a second order method that increases the accuracy of the solution for discontinuous problems (*e.g.* uniform distributions) by introducing gradient limiters. We considered a range of grids to analyse the convergence of the two finite volume methods. The initial grid had eight cells in the x direction and 12 cells in the z direction. The time increment for a given grid was set to $\Delta t = 0.5\Delta x/e_0$, based on the Courant number. The number of cells in the angle dimension is determined $\Delta\alpha = g_0\Delta t/0.5$. Thinner grids were obtained by dividing cell dimensions by two, until the number of cells reached 64 cells in the x dimension and 96 cells in the z dimension.

Analytical models, finite volume methods and CDPM simulations were initiated using root apical meristem distributions consisting of a circular envelope with a median radius of 2 cm and a thickness of 3 cm. The radial distribution was either uniformly distributed or normally distributed with mean 2 cm and standard deviation 0.5 cm. The distribution of root angles on this domain varied in the interval $[-\pi/5, 0]$ for root tips at the surface and in the interval $[-\pi/2, -\pi/2+\pi/5]$ on the vertical plane. The interval for root angle for the remaining positions was linearly interpolated as a function of the zenith angle defining their position on the hemisphere. Models using no gravitropic rate ($g_0 = 0$) or high gravitropic rate ($g_0 = 0.3$) were simulated. Simulation time used for validation corresponds to 3 days of growth. Total soil volume was assumed to be 10 cm by 15 cm by $\pi/2$.

Simulation results were used to build spatial maps of the root apical meristem density distribution and maps of the root length density distribution. Next, root densities from CDPMs and analytical models were mapped onto the same regular grid as that used by finite volume methods and compared using Eq. (25). Mapping of CDPMs used Eq. (12). Errors between numerical methods (CDPM and both finite volume methods) and analytical solutions were recorded for each combination of grid size, gravitropic rate and initial conditions. Error and computation time were plotted as a function of grid size. Variations, induced by changes in initial conditions and gravitropic rate, were plotted as intervals around mean error curves for a given grid size (see Fig. 5).

2.6. A simple case of crop–weed competition

CDPMs can be applied to predict the behaviour of ensembles of plants in a patch of soil. In order to illustrate the use of CDPMs for such applications, we used the model presented in Section 2.2 to analyse spatio-temporal patterns of root competition intensity in a simple crop–weed system (Fig. 3A). In a system where two plant types coexist, we can define a partition (I_c, I_w) of the set of plants, so that $I_c \cup I_w = \{1, \ldots, s\}$. Using the root length density mixture vector of Eq. (16), we derived the root length density of crop plants $l_c = \sum_{p \in I_c} l^p$. The root length density of weed plants followed: $l_w = \sum_{p \in I_w} l^p$. The fraction of soil ϕ accessed by roots in a unit volume of soil is a non-decreasing function of root length density and tends towards a maximum value of 1. The increase slows down gradually as roots occupy a larger volume of soil. In order to understand the definition of proportional resource capture, it is useful to consider the region of soil accessed by a portion of root as a cylinder of radius r_c of length dl. If the fraction of soil accessible to roots is ϕ, then the probability of the new portion of root to enter a new region of soil is $(1-\phi)\pi r_c^2$. The increase of the fraction of soil accessible per unit added root length density can therefore be expressed using the following equation:

$$\frac{d\phi}{dl} = (1-\phi)\pi r_c^2. \tag{26}$$

The solution to this equation is $\phi = 1 - e^{-\pi r_c^2 l}$. This modelling concept is termed the principle of proportional resource capture. In real conditions, the domain of soil available is unknown, but similar relations between root length density and soil fraction accessible are observed (King et al., 2003). Application of the principle of proportional resource capture to crop–weed mixtures is therefore expressed as

$$\phi = 1 - e^{-\kappa(l_c + l_w)}, \tag{27}$$

where κ (cm^2) is the resource capture coefficient and ϕ is the fraction of soil accessible to plant roots. The fraction of soil ϕ_c accessed by crop plants only is then proportional to the fraction of crop roots in soil

$$\phi_c = l_c\phi/(l_c + l_w). \tag{28}$$

The intensity of competition is then quantified as the fraction of crop roots that becomes redundant due to competition and is termed Root

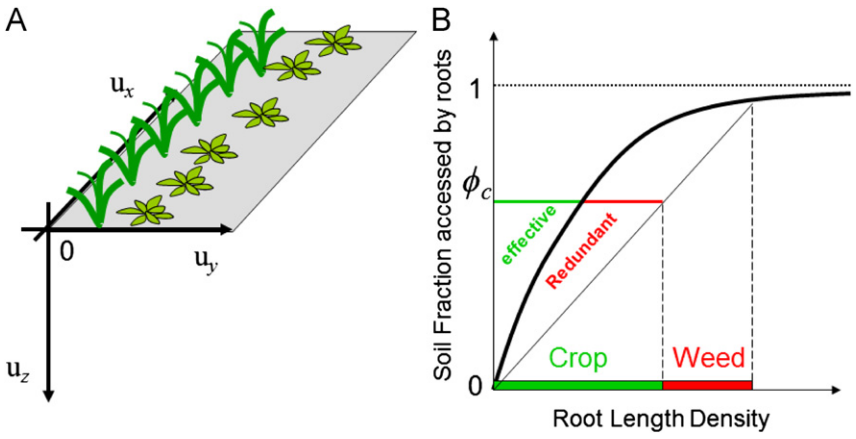

Fig. 3. (A) A simple case of crop–weed underground competition. Crop and weed plants were placed in two parallel rows. Position of the weeds included a random deviation in the x-axis. (B) The competition intensity is quantified using the principle of proportional resource capture (King et al., 2003): ϕ, the fraction of soil volume accessed by roots (y-axis), increases as a function of root length density (x-axis) towards a maximum value 1. This increase slows down gradually as the probability that a crop root enters a fraction of soil free of roots is reduced. In the case of a mixture, the fraction of soil available to a crop (ϕ_c) is proportional to the crop vs. weed root length density ratio (respectively, green and red bars on the x-axis). However, the same fraction of soil, in the absence of competition, could be obtained with fewer roots (green bar labelled 'effective'). The remaining fraction of produced crop root remains unused (red bar labelled 'redundant'). The intensity of competition can be quantified as the ratio of redundant root length density over total root length density, and is termed the Root Redundancy Index (Eq. (29)). (For interpretation of the references to color in this figure caption, the reader is referred to the web version of this article.)

Redundancy Index (RRI) (see Fig. 3B)

$$\mathrm{RRI} = 1 - \frac{\log(1-\phi_c)}{\kappa l_c}. \quad (29)$$

The growth model used to represent the crop plants was derived from a previous work on Barley (*Hordeum vulgare* L. cv. Optic) with growth rate numerical values equal to those fixed after Eqs. (17). The model was calibrated from minirhizotron data at establishment stage, and showed good correlation with measurement data (Dupuy et al., 2010). Crop plants were virtually sown along a row in the y-direction every 4 cm. The model for weed plants was based on data collected on common lambsquarters (*Chenopodium album*) and velvetleaf (*Abutilon theophrasti* Medicus) weeds by Seibert and Pearce (1993). Elongation rate and branching rate were obtained by fitting a simple analytical model linking elongation rate and branching rate to total root length: $\int l(t)\,dV = b_0 e_0 \exp(b_0 t)$ ($e_0 = 1.5$ cm day^{-1} and $b_0 = 0.3$ day^{-1}) ($g_0 = 0$). We neglected the gravitropic rate of weeds because data was not available. Also common lambsquarters and velvetleaf, like most dicotyledon plants, have their root system constituted mostly of weakly gravitropic secondary lateral roots. Weeds were placed randomly around an average line parallel to the row of crops. Simulations ran for 12 days of growth after emergence. 3D plant domains used grids subdivided into 10 sub-domains along the ϕ coordinate lines (zenith angle) and 5 in the R (radial) and α (root angle) coordinate lines.

3. Results and discussion

3.1. Accuracy and convergence of CDPMs

Solutions to Eq. (1) form propagating waves of apical meristem density where velocity is given by x_0 and z_0 in Eqs. (22). The plot of solutions obtained with Taylor series illustrates this result (Fig. 4A and B, leftmost column). A plant root system, defined as the footprint of this wave (time integration of the apical meristem density), forms a growing domain of non-zero root length density. Results obtained by the different numerical methods (upwind, minmod and CDPMs in Fig. 4, respectively, second, third and fourth columns) reproduced the same mechanisms. The upwind scheme was the least accurate numerical scheme; solutions were significantly smoothed in comparison to the analytical solution. Minmod approach improved considerably this problem and the solution obtained was qualitatively similar to CDPMs.

In Fig. 5, we compared the accuracy of numerical methods using plots of error and computation time as a function of the number of elements per mesh. Results showed that both upwind

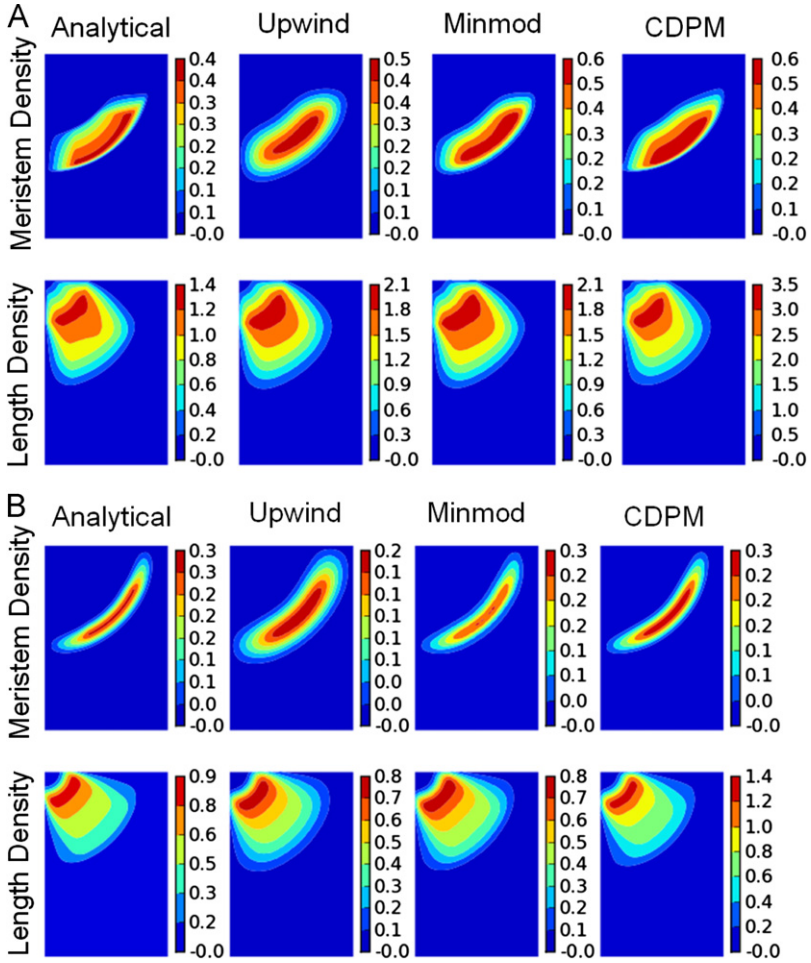

Fig. 4. Comparison of CDPMs with analytical solutions and two standard finite volume methods (upwind and upwind with minmod flux limiter). The first column shows the analytical solution in Eq. (21). The second column shows results of the upwind scheme, which is a first order method suitable to simulate wave propagation mechanisms. The third column shows the results from the upwind scheme with minmod scheme, which is a second order method. The fourth column presents the CDPM results. Solutions are presented for root tips and root length density distributions for two different initial conditions and gravitropic rate values. Results shown are for the highest resolution grids tested in our simulations. Colours scale from blue for low densities to red for high densities. (A) Gravitropic rate of 0.3 s^{-1} and uniform initial distribution. (B) Gravitropic rate of 0 s^{-1} and Gaussian initial distribution. (For interpretation of the references to color in this figure caption, the reader is referred to the web version of this article.)

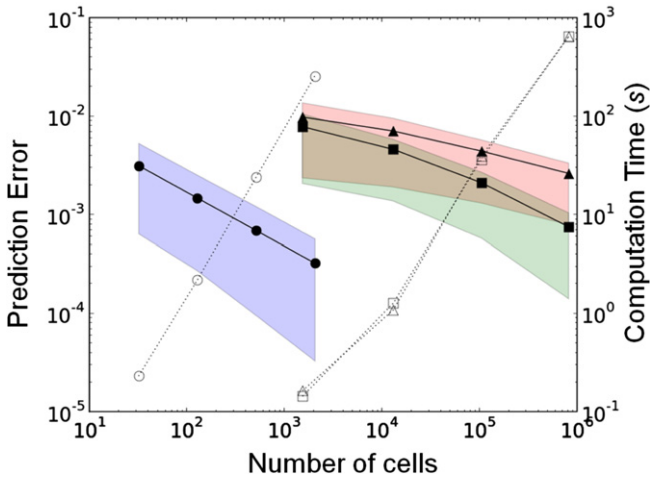

Fig. 5. Root length density prediction error (plain solid line) and computational time (dotted line) of CDPM (circle), upwind (triangle) and minmod (square) finite volume methods as a function of the number of cells in the grid. Plain lines represent the mean error and the corresponding shades represent lower and higher bounds of the error. Although the CDPM is converging linearly (log–log scale) towards the exact solution, the number of cells required for a good approximation to be obtained is lower than classical finite volume methods. Computational time per cell in the grid is higher for the CDPM but overall, in the range of computational time allowed by a desktop PC (with a 2.2 GHz processor and 2 GB memory), accuracy levels obtained by the CDPM were better than those obtained by finite volume methods.

and CDPM methods, described in Section 2 converged linearly (in log-log scale) towards the correct solution whereas the minmod method had a quadratic convergence, which is consistent with second order method behaviour. Amongst the methods presented to numerically solve Eq. (1), CDPMs outperformed finite volume methods of first (upwind) and second (minmod) order in terms of absolute prediction error and computation time: best mean prediction error with CDPMs was 0.0002 compared to 0.0007 for the minmod method and 0.0015 for the upwind method. At an error of 0.002, computation time is 0.15 s with CDPMs and required, respectively, 5 s and 15 s for minmod and upwind methods. Trends in the log–log scale indicate that the minmod method could perform better than CDPMs for grids of higher resolution than those tested. However, simulations for grids of this type would require computation times several orders of magnitude longer and not attainable in most realistic scenarios.

Several factors made CDPMs more accurate than finite volume methods. First, CDPMs use grids that correspond to the volume occupied by plants only. Finite volume methods, on the opposite, are forced to use fixed grids that either cover large regions of the generalised space E and can involve intractable computations. Because generalised spaces have increased dimensions, the gain obtained by CDPMs is significant. Secondly, fixed grids are sensitive to initial conditions (Meister and Struckmeier, 2002). In general plant models are initiated at seeds which occupy a vanishing fraction of the soil domain. As a consequence, initial conditions are usually ill-defined using such meshes. Although fixed grid methods can be suitable to model root systems at later stage of development, their accuracy is hindered by highly inconsistent definition of initial conditions. In contrast, CDPM grids adapt to the actual size of the root domain. CDPMs can therefore be initiated with fine mesh concentrated on the seed, and an expansion can occur during the growth of the root system. This property allows CDPMs to perform simulations over longer growth periods. Finally, the computation of fluxes to update root densities in fixed grids is prone to numerical diffusion (Chock, 1991). In CDPMs, apical trajectories were used to deform the grid, and diffusion was only introduced in the tangential direction due to fluxes through side faces (see Fig. 2). However, results showed that the root density computation time per cell in CDPMs was higher than that of finite volume methods. It indicates that algorithms for the computation of fluxes between deformed side faces (Fig. 2B) could be enhanced. Future work must now address this issue.

Accuracy and convergence of numerical simulations are important properties to examine, when constructing predictive models. However, there are numerous other factors that contribute to the making of a useful modelling tools. In biological applications in particular, numerical errors are rarely the main source of loss of accuracy. Other sources of error include inadequacy of the mathematical model to represent the nature of the biological system. In many cases, this is due to the lack of mechanistic understanding of the processes under scrutiny or the difficulty to collect suitable data. Many root architectural parameters are difficult to estimate *in situ* (De Smet et al., 2012). For these reasons, models with minimal parameter sets, that can be applied to field data *e.g.* obtained by soil coring or minirhizotron, are now receiving greater attention from the community. In our model, there is a direct relation between root growth parameters, *e.g.* branching angle, gravitropic rate and branching rate, and spatial mappings of root length density. This property will be essential in the future to parametrise model on field data. The improved calculation time provided by CDPMs will allow setting parameter through non-linear optimisation algorithm, with the advantage over classic exponential models (Page and Gerwitz, 1974; King et al., 2003), that parameters can be obtained on two or three dimensional mappings of root length density.

3.2. Modelling plant populations and competition using density based models

Because CDPMs drastically improved global computation efficiency, it was possible to use them in a simple case of crop–weed competition. Using the principle of proportional resource capture, we derived a measure of the competition intensity between crops and weeds: the Root Redundancy Index (RRI see Eq. (29) and Fig. 3B). The RRI is the fraction of roots that is produced but does not have access to resources due to competition. When no weed is present, the RRI is constant for any value of the crop root length, and is equal to 0. When weed root length density increases, competition gets more intense for higher values of crop root length density; the RRI increases with crop root length density as a sigmoid-shaped function (Fig. 6A). At a constant weed root length density, the resource capture coefficient has limited impact on the RRI vs. crop root length relationship. The relationship is approximately linear, and the increase in resource capture coefficient induces a shift in the RRI (Fig. 6B). This phenomenon expresses the expected increase in the probability that a crop root is in the zone of influence of weed roots when crop root zone of influence is increased.

The RRI was used to visualise the spatial distribution of the competition intensity in the field. We observed that two contrasting root systems induced localised and intensive zones of competition (Fig. 7). In our simulations, significant competition occurred at levels close to the surface and between the two rows, where, respectively, a root type and its competitor were sown. Fig. 7 illustrates this pattern of competition: at 5 cm depth, there was a large overlap between the two root types (Fig. 7A), which involved a nearly twofold increase in root length density and subsequent changes in RRI. However, this overlap rapidly decreased with depth (Fig. 7B). This effect, albeit diminishing with depth, was still observed in the entire region where weed roots had developed, not only at the imaginary boundary between the two plants.

This study case showed that more effective density-based models can be constructed and used when the number of plants in a system (s) is large (Fig. 8). Finite volume simulations of such

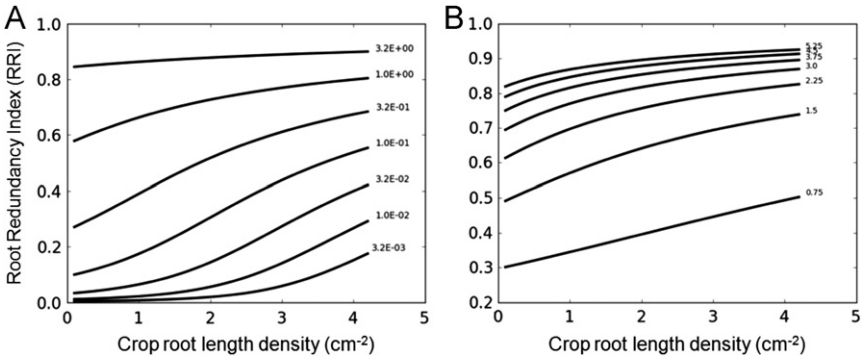

Fig. 6. Changes of the Root Redundancy Index (RRI) as a function of crop root length for (A) different values of weed root length L_w (resource capture coefficient κ set to 2 cm^2) and (B) different values of resource capture coefficient κ (L_w set to 1 cm^{-2}). (A) At a given level of weed root length density, the RRI is an increasing function of the crop root length density (L_c). At low competition levels the RRI is significant only at high crop root length density. At high competition levels the RRI is nearly constant at any crop root length density level. (B) An increase in κ induces a uniform increase in the RRI with limited non-linearity.

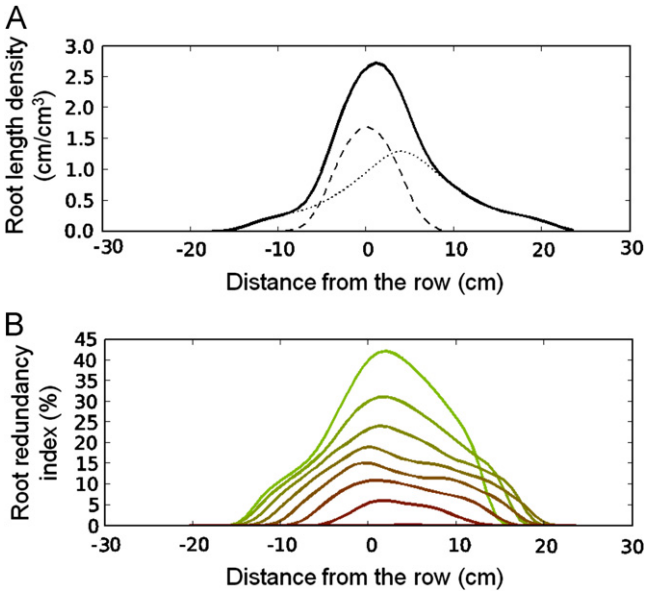

Fig. 7. (A) Variation of the total root length density along an axis perpendicular to the row of crops at 5 cm depth. The bold line represents the total root length density of the mixture. The dashed line represents the crop root length density and the dotted line represents the root length density of weeds. (B) Root Redundancy Index (RRI) along an axis perpendicular to the row of crops and taken at 2 cm depth intervals from 5 cm (green) to 19 cm (brown) depth. (For interpretation of the references to color in this figure caption, the reader is referred to the web version of this article.)

scenarios would require the number of variables defined at each cell to increase linearly as a function of s. When the number of plants increases, the grid size is also required to grow proportionally to s. The complexity of computations would therefore expand proportionally to s square *i.e.* $O(s^2)$. In the case of CDPMs however, the number of cells in the grid increases as a linear function of the number of plants in the simulation but each cell of a model defines the root density of a unique plant. Therefore, computations with CDPMs have complexity $O(s)$.

The implementation of root–root interactions is also greatly facilitated with the CDPM approach. Single plants are identified as independent physical entities, and only plants in contact with each other are allowed to interact during the simulation. For example, it is possible to determine interacting domains using Delaunay triangulation or K-nearest neighbours methods (Moeur, 1993). This reduces the number of candidate neighbours to test for spatial interactions, and complexity is reduced to $O(s)$. A fully connected network of interaction would have complexity $O(s^2)$.

3.3. New opportunities for modelling plant–environment interactions

Plants grow complex architectures in order to explore space and acquire resources efficiently. Models provide essential information to understand the complex functions of plant architectures. Early models in the 1970s introduced density-based approaches to study root and shoot growth (Charles-Edwards and Thornley, 1973; Gerwitz and Page, 1974; Lang and Shell, 1975). However, density models lacked suitable descriptions of plant geometry, and showed limitations in the study of spatial processes. With the advent of more powerful computers, architectural models have come to dominate the field (Prusinkiewicz, 2004; Barczi et al., 2008). For example, architectural models have been essential to understand the role of canopy structure on light interception (Pearcy and Yang, 1996; Rey et al., 2008), or to identify regions of soil with high root uptake (Lynch and Brown, 2002; Dunbabin et al., 2004; Doussan et al., 2006).

Nevertheless, architectural models are not adapted to cases where ensembles of plants are interacting and competing for resources in a field. To study processes at this scale, a new generation of simplified, but still accurate plant models must be developed. In some cases, a representation of space is simply not required at all. For example, in the case of phosphate uptake by root system, it was shown that mobility through convection and diffusion can be neglected and total root length alone is sufficient to predict phosphate acquisition (Leitner et al., 2010). In many other cases however, the architectural properties must be incorporated into models. Experience from other fields of research have demonstrated that, in this case, Partial Differential Equations provide a powerful framework to derive simplified models. Models for tip growth in a fungal network were successfully used in the past (Edelstein-Keshet and Ermentrout, 1989; Nopharatana et al., 1998). More recent approaches now integrate growth and resource uptake from soil (Schnepf and Roose, 2006; Schnepf et al., 2008). In biomedical sciences, similar approaches have been developed to understand and predict the growth of angiogenesis and tumors (Anderson and Chaplain, 1998). The use of oriented distribution function in PDE is also common in models of blood flow (Vankan et al., 1996) and theoretical chemistry (Solc and Stockmayer, 1970).

Simplifications can also be achieved through a better understanding of how space is explored by the plant architecture. It could be generically described as the plant's zone of influence (ZOI). The concept of ZOI is not a new concept in ecology (Cescatti, 1997) and agronomy (Hammer et al., 2009) and has been used to formalise plant–environment interfaces. However, plants' ZOIs are generally dynamic and complex traits. They expand throughout a plant life cycle but such expansion is constrained by biological and physical

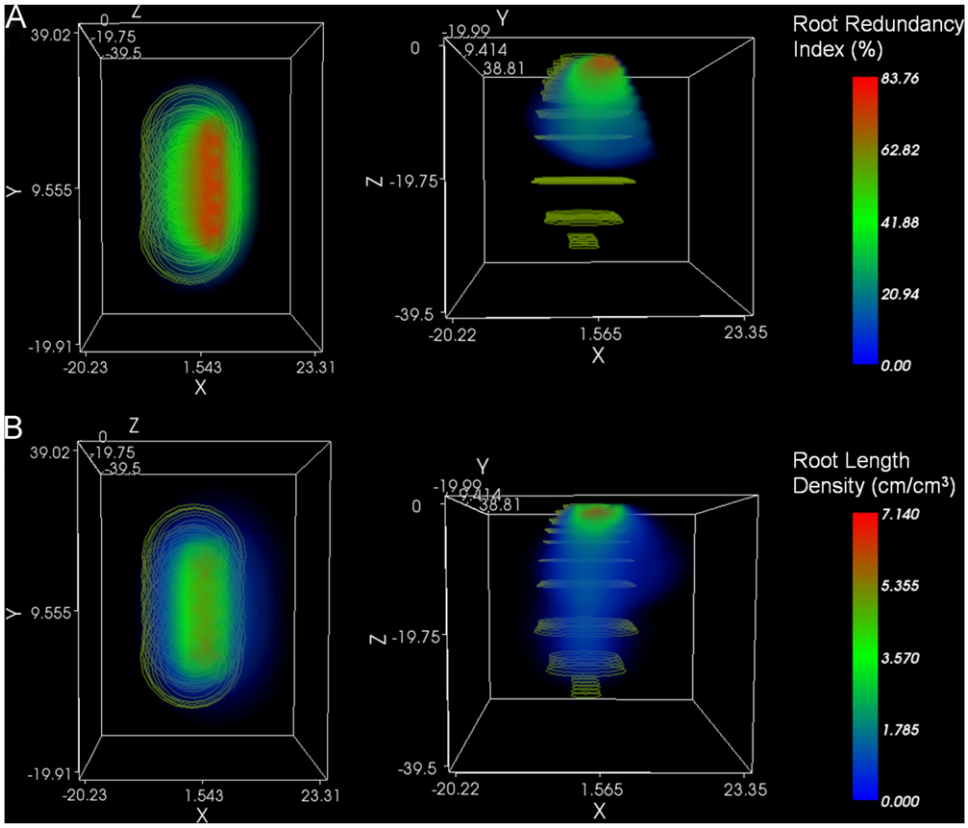

Fig. 8. 3D representation of the spatial distribution of (A) Root Redundancy Index (RRI) and (B) total root length density of the mixture. Graphs on the left represent the row of crops viewed from the top and those on the right represent the same row viewed from the side. Yellow circles outline the domain occupied by each crop in the row. (For interpretation of the references to color in this figure caption, the reader is referred to the web version of this article.)

factors *e.g.* mechanical (Niklas and Spatz, 2004) and hydraulic (Sperry et al., 2008). Previous studies lacked theoretical foundations to mechanistically model ZOIs (Weiner and Damgaard, 2006; Pachepsky et al., 2001).

Our results showed that plants ZOIs can be predicted based on plants elementary developmental processes. We also showed that the ZOI is more than a geometrical trait. It must include a description of how plant organs are distributed across the plant domain. This can be obtained as the solution of growth equations in terms of density functions. Although we focused on root system modelling, the method we presented could be modified to describe shoot development. Necessary modifications include replacement of length density by leaf area density with elongation rate being expressed in area per second. The gravitropic coefficient would also need be replaced by more complex functions to account for bending of branches due to weight and phototropism.

4. Conclusion

This study developed a first generation algorithm for the simulation of the growth of root systems. It was possible to describe root density distributions within domains that grow as a result of root elongation and branching processes. We were also able to provide more accurate and faster predictions, than classical numerical methods. Numerous applications are anticipated, particularly when ensembles of plants are competing in a field. Challenges remain to optimise simulation algorithms, both for the discretisation and approximation of solutions on such domains. Fortunately, the abundant literature on numerical methods for solving differential equations indicates potential clues for improvements.

List of symbols

Coordinate systems

$\mathbf{m}=(x,y,z)$	spatial coordinates
t (day)	time
r (cm)	radial coordinate in the spherical coordinate system
θ,φ	azimuth and zenith angles in spherical coordinate system
α	angle of root inclination (gravitropic angle)
β	angle of root azimuth (plagiotropic angle)
$\mathbf{M}=(R,\theta,\varphi,A)$	semi-Lagrangian root coordinates in generalised space
$\mathbf{u_x},\mathbf{u_y},\mathbf{u_z}$	basis in Cartesian coordinate system
$\mathbf{u_r},\mathbf{u}_\theta,\mathbf{u}_\varphi$	basis in spherical coordinate system

Root quantities

ρ_a (cm^{-3})	distribution of apical meristem density
ρ_l (cm^{-2})	distribution of root length density
ρ_b (cm^{-3})	distribution of branching density
b ($\mathrm{cm}^{-3}\,\mathrm{day}^{-1}$)	volumetric root branching rate
e ($\mathrm{cm\,day}^{-1}$)	root expansion rate
g (day^{-1})	root tropic rate
h (day^{-1})	root plagiotropic rate
ϕ	proportional resource capture
κ	resource capture coefficient

Discretisation

n	number of cells in the grid of a plant
s	number of plants

$_{i,j,k}$	subscript indices indicate cell position in the grid
$^{p,\tau,*}$	superscript indices indicate whole plant attribute
C_i	ith cell of a grid
Q_i	number of root apical meristem in the ith cell
$\mathbf{M}_i=(R_i,\theta_i,\varphi_i,A_i)$	position of the ith cell of the grid
$t,\Delta t,\tau$	time, time increment and time step
$\Delta\Theta,\Delta\varphi,\Delta R,\Delta A$	size a grid cells

Crop–weed interactions

I_c,I_w	indices for crop/weed in an ensemble of plants
$\mathbf{l}$	root length density mixture vector
l_c,l_w	total crop/weed root length in a cell

Acknowledgements

We are grateful to Glyn Bengough, Tim Daniell, Mark Young and Philip White for valuable comments on the manuscript. The James Hutton Institute receives support from the Scottish Government Rural and Environment Science and Analytical Services (RESAS, Workpackage 3.3) Division.

References

Acock, B., Pachepsky, Y., 1996. Convective-diffusive model of two-dimensional root growth and proliferation. Plant Soil 180, 231–240.
Anderson, A., Chaplain, M., 1998. Continuous and discrete mathematical models of tumor-induced angiogenesis. Bull. Math. Biol. 60, 857–899.
Barczi, J.-F., Rey, H., Caraglio, Y., de Reffye, P., Barthelemy, D., Dong, Q.X., Fourcaud, T., 2008. Amapsim: a structural whole-plant simulator based on botanical knowledge and designed to host external functional models. Ann. Bot. 101, 1125–1138.
Bastian, P., Chavarria-Krauser, A., Engwer, C., Jaeger, W., Marnach, S., Ptashnyk, M., 2008. Modelling in vitro growth of dense root networks. J. Theor. Biol. 254, 99–109.
Cescatti, A., 1997. Modelling the radiative transfer in discontinuous canopies of asymmetric crowns. I. Model structure and algorithms. Ecol. Model. 101, 263–274.
Charles-Edwards, D.A., Thornley, J.H.M., 1973. Light interception by an isolated plant: a simple model. Ann. Bot. 37, 919–928.
Chock, D.P., 1991. A comparison of numerical methods for solving the advection equation. Atmos. Environ. 25, 853–871.
De Smet, I., White, P.J., Bengough, A.G., Dupuy, L., Parizot, B., Casimiro, I., Heidstra, R., Laskowski, M., Lepetit, M., Hochholdinger, F., Draye, X., Zhang, H., Broadley, M.R., Péret, B., Hammond, J.P., Fukaki, H., Mooney, S., Lynch, J.P., Nacry, P., Schurr, U., Laplaze, L., Benfey, P., Beeckman, T., Bennett, M., 2012. Analyzing lateral root development: how to move forward. Plant Cell 24, 15–20.
de Willigen, P., Heinen, M., Mollier, A., Van Noordwijk, M., 2002. Two-dimensional growth of a root system modelled as a diffusion process. 1. Analytical solutions. Plant Soil 240, 225–234.
Doussan, C., Pierret, A., Garrigues, E., Pagès, L., 2006. Water uptake by plant roots: Ii—modelling of water transfer in the soil root-system with explicit account of flow within the root system—comparison with experiments. Plant Soil 283, 99–117.
Draye, X., Kim, Y., Lobet, G., Javaux, M., 2010. Model-assisted integration of physiological and environmental constraints affecting the dynamic and spatial patterns of root water uptake from soils. J. Exp. Bot. 61, 2145–2155.
Dunbabin, V., Rengel, Z., Diggle, A., 2004. Simulating form and function of root systems: efficiency of nitrate uptake is dependent on root system architecture and the spatial and temporal variability of nitrate supply. Funct. Ecol. 18, 204–211.
Dupuy, L., Vignes, M., McKenzie, B., White, P., 2010. The dynamics of root meristem distribution in soil. Plant Cell Environ. 33, 358–369.
Edelstein-Keshet, L., Ermentrout, B., 1989. Models for branching networks in two dimensions. SIAM J. Appl. Math. 49, 1136–1157.
Fourcaud, T., Zhang, X., Stokes, A., Lambers, H., Körner, C., 2008. Plant growth modelling and applications: the increasing importance of plant architecture in growth models. Ann. Bot. 101, 1053–1063.
Ge, Z., Rubio, G., Lynch, J., 2000. The importance of root gravitropism for inter-root competition and phosphorus acquisition efficiency: results from a geometric simulation model. Plant Soil 218, 159–171.
Gerwitz, A., Page, E., 1974. An empirical mathematical model to describe plant root systems. J. Appl. Ecol. 11, 773–781.
Hammer, G.L., Dong, Z., McLean, G., Doherty, A., Messina, C., Schussler, J., Zinselmeier, C., Paszkiewicz, S., Cooper, M., 2009. Can changes in canopy and/or root system architecture explain historical maize yield trends in the U.S. corn belt? Crop Sci. 49, 299–312.
King, J., Gay, A., Sylvester-Bradley, R., Bingham, I., Foulkes, J., Gregory, P., Robinson, D., 2003. Modelling cereal root systems for water and nitrogen capture: towards an economic optimum. Ann. Bot. 91, 383–390.
Lang, A.R.G., Shell, G.S.G., 1975. Sunlight areas and angular distributions of sunflower leaves for plants in single and multiple rows. Agric. Meteorol. 16, 5–15.
Leitner, D., Schnepf, A., Klepsch, S., Roose, T., 2010. Comparison of nutrient uptake between three-dimensional simulation and an averaged root system model. Plant Biosyst. 144, 443–447.
Leveque, R.J., 2002. Finite Volume Methods for Hyperbolic Problems. Cambridge Texts in Applied Mathematics. Cambridge University Press, Cambridge.
Lucas, M., Laplaze, L., Bennett, M.J., 2011. Plant systems biology: network matters. Plant Cell Environ. 34, 535–553.
Lynch, J., 2007. Roots of the second green revolution. Aust. J. Bot. 55, 493–512.
Lynch, J., Brown, K., 2002. Topsoil foraging—an architectural adaptation of plants to low phosphorus availability. Plant Soil 237, 225–237.
Mattheij, R.M.M., Rienstra, S.W., ten Thije Boonkkamp, J.H.M., 2005. Partial Differential Equations: Modeling, Analysis, Computation. Society for Industrial and Applied Mathematics, Philadelphia.
Meister, A., Struckmeier, J., 2002. Hyperbolic Partial Differential Equations: Theory Numerics and Applications. Friedrich Vieweg & Sohn Verlag, Braunschweig.
Moeur, M., 1993. Characterizing spatial patterns of trees using stem-mapped data. For. Sci. 39, 756–775.
Niklas, K.J., Spatz, H.-C., 2004. Growth and hydraulic (not mechanical) constraints govern the scaling of tree height and mass. Proc. Natl. Acad. Sci. U.S.A. 101, 15661–15663.
Nopharatana, M., Howes, T., Mitchell, D., 1998. Modelling fungal growth on surfaces. Biotechnol. Tech. 12, 313–318.
Pachepsky, E., Crawford, J.W., Bown, J.L., Squire, G., 2001. Towards a general theory of biodiversity. Nature 410, 923–926.
Page, E.R., Gerwitz, A., 1974. Mathematical models, based on diffusion equations, to describe root systems of isolated plants, row crops, and swards. Plant Soil 41, 243–254.
Pagès, L., Vercambre, G., Drouet, J.L., Lecompte, F., Collet, C., Le Bot, J., 2004. Root type: a generic model to depict and analyse the root system architecture. Plant Soil 258, 103–119.
Pearcy, R.W., Yang, W., 1996. A three-dimensional crown architecture model for assessment of light capture and carbon gain by understory plants. Oecologia 108, 1–12.
Prusinkiewicz, P., 2004. Modeling plant growth and development. Curr. Opin. Plant Biol. 7, 79–83.
Reddy, V., Pachepsky, Y.A., 2001. Testing a convective–dispersive model of two-dimensional root growth and proliferation in a greenhouse experiment with maize plants. Ann. Bot. 87, 759–768.
Rey, H., Dauzat, J., Chenu, K., Barczi, J.-F., Dosio, G.A.A., Lecoeur, J., 2008. Using a 3-D virtual sunflower to simulate light capture at organ, plant and plot levels: contribution of organ interception, impact of heliotropism and analysis of genotypic differences. Ann. Bot. 101, 1139–1151.
Schnepf, A., Roose, T., 2006. Modelling the contribution of arbuscular mycorrhizal fungi to plant phosphate uptake. New Phytol. 171, 669–682.
Schnepf, A., Roose, T., Schweiger, P., 2008. Growth model for arbuscular mycorrhizal fungi. J. R. Soc. Interface 5, 773–784.
Seibert, A.C., Pearce, R.B., 1993. Growth analysis of weed and crop species with reference to seed weight. Weed Sci. 41, 52–56.
Solc, K., Stockmayer, W., 1970. Kinetics of diffusion-controlled reaction between chemically asymmetric molecules. I. General theory. J. Chem. Phys. 54, 2981–2988.
Sperry, J.S., Meinzer, F.C., McCulloh, K.A., 2008. Safety and efficiency conflicts in hydraulic architecture: scaling from tissues to trees. Plant Cell Environ. 31, 632–645.
Stokes, A., Atger, C., Bengough, A., Fourcaud, T., Sidle, R., 2009. Desirable plant root traits for protecting natural and engineered slopes against landslides. Plant Soil 324, 1–30.
Tsegaye, T., Mullins, C., Diggle, A., 1995. An experimental procedure for obtaining input parameters for the rootmap root simulation program for peas (*Pisum sativum* l). Plant Soil 172, 1–16.
Vankan, W.J., Huyghe, J.M., Janssen, J.D., Huson, A., 1996. Poroelasticity of saturated solids with an application to blood perfusion. Int. J. Eng. Sci. 34, 1019–1031.
Weiner, J., Damgaard, C., 2006. Size-asymmetric competition and size-asymmetric growth in a spatially explicit zone-of-influence model of plant competition. Ecol. Res. 21, 707–712.
Wiegers, B.S., Cheer, A.Y., Silk, W.K., 2009. Modeling the hydraulics of root growth in three dimensions with phloem water sources. Plant Physiol. 150, 2092–2103.
Wu, L., McGechan, M.B., McRoberts, N., Baddeley, J.A., Watson, C.A., 2007. Spacsys: integration of a 3D root architecture component to carbon, nitrogen and water cycling-model description. Ecol. Model. 200, 343–359.
Zhang, K., Greenwood, D., White, P., Burns, I., 2007. A dynamic model for the combined effects of N, P and K fertilizers on yield and mineral composition; description and experimental test. Plant Soil 298, 81–98.
Zienkiewicz, O.C., Taylor, R., 1998. The Finite Element Method. McGraw-Hill, London/New York.